21st European Conference on Fracture, ECF21, 20-24 June 2016, Catania, Italy

Two-parameter fracture characterization of a welded pipe in the presence of residual stresses

S. Abolfazl Zahedi*, Andrey Jivkov

School of Mechanical, Aerospace and Civil Engineering, The University of Manchester, Manchester, M13 9PL, UK

Abstract

In this paper two-parameter fracture characterization of elastic and elastic-plastic stress/strain field around a crack front is presented for a welded pipe component containing a circumferential through-thickness crack. A macro function programmed in PYTHON is used to compute the constraint parameters (T-stress, T_z and Q factors) of the specimen in the open source finite element package Code_Aster. Data obtained from literature was employed to support three-dimensional finite element models developed in this research to study the impact of high magnitude repair-weld residual stresses. Complete distributions of the T-stress, T_z and Q-factors were obtained along a 3D crack front in the presence of residual stresses. The effects of stresses (residual and operational) on the constraint parameters are studied. It is shown that a two-parameter methodology provides effective characterization of three dimensional elastic–plastic crack tips constraint.

Peer-review under responsibility of the Scientific Committee of ECF21.

Keywords: constraint parameters; T-stress; T_z-factor; Q-factor; residual stress

1. Introduction

Residual stresses are present in most mechanical or thermal components due to the fabrication methodology, such as welding. They attract considerable attention in engineering applications, because of their impact on part distortion, service performance and the costs associated with failures (Gannon et al., 2010). Therefore, it is necessary to understand the combined effect of mechanical loading and residual stresses on the fracture of structures in order to provide a more accurate structural integrity assessment. The prediction of crack initiation and propagation requires

* Corresponding author. Tel.: +44-0161-306-2737; fax: +44-0161-306-2737.
E-mail address: Abolfazl.Zahedi@manchester.ac.uk

Peer-review under responsibility of the Scientific Committee of ECF21.

taking into account the three-dimensional nature of the crack-front stress field, which is depended on the loading conditions and crack geometry. It is well known that the elastic or plastic fracture mechanics by considering the stress intensity factor K or the J-integral parameters works well only under high constraint conditions. Differently, constant stress contributions acting over a longer distance from the crack tip affect fracture mechanics properties (Kim and Paulino, 2003).

For cracks under low constraint conditions, the crack-tip stress field deviates from small scale yielding (SSY) solution. To quantify this effect for elastic or elastic-plastic behaviour, additional parameters to the stress intensity factor K or the J-integral are required. In a two-parameter approach, the first parameter measures the degree of crack-tip deformation, as characterized by K or J-integral and the second parameter characterizes the degree of crack tip constraint. In elastic materials this is the second distance-independent term of the Williams expansion for stresses, namely the T-stress in mode I and mixed-mode in-plane loading. This parameter has a significant effect on the size and shape of the plastic zone developing around the crack tip. For three-dimensional cracked bodies, the constraint effect through the thickness is evaluated by the T_z-factor. In elastic-plastic materials a non-dimensional Q-factor quantifies the level of deviation of a stress/strain field from a SSY solution.

The application of two-parameter fracture mechanics, K-T or J-Q, to include the constraint effect in the engineering assessment procedure is becoming more and more established. Meanwhile, the effects of residual stresses on the crack driving forces, and the stress field near the crack-tip in integrity assessments are still unexplored in the open literature. Hill and Panontin (1998) investigated the effects of residual stresses on ductile and brittle crack growth initiation in a pipe with a circumferential crack, and confirmed that residual stresses contribute to the crack driving forces. Hill and Yau (2000) studied the effects of thermo-mechanical loading and residual stresses on crack-tip constraints. Liu et al. (2008) computed the crack-tip constraint for single edge notched specimens subject to an external bending load in a condition of one-dimensional residual stress field. Farhani and Sattari-Far (2011) presented the effects of residual stresses on crack behaviour in a large disk shaped model. All these studies were limited to a small number of crack geometries and loading cases in the presence of residual stresses. It is of practical interest to consider a body with a more complex shape under primary and secondary stresses to calculate the fracture constraint parameters along the crack front.

In this study T-stress, T_z and Q factors are computed for a welded pipe component made with austenitic stainless steel containing a circumferential through-thickness crack. Since welds made from this material cannot be normally post-weld heat treated before entering service, the pipe will contain weld residual stresses. A macro function programmed in PYTHON is used to compute constraint parameters (T-stress, T_z and Q factors) in the open source finite element package Code_Aster.

2. Theory

2.1. Computation of T-stress and T_z factor

Based on isotropic linear elasticity theory, when an elastic cracked body is subjected to external forces (see Fig.1) the stress field in the vicinity of a crack tip can be expressed by Williams' expansion. The stresses near the crack-tip can be written as follows (Novotný, 2012):

$$\sigma_{rr} = \frac{K_I}{\sqrt{2\pi r}}\left(\frac{5}{4}\cos\frac{\theta}{2} - \frac{1}{4}\cos\frac{3\theta}{2}\right) + \frac{K_{II}}{\sqrt{2\pi r}}\left(-\frac{5}{4}\sin\frac{\theta}{2} + \frac{3}{4}\sin\frac{3\theta}{2}\right) + T\cos^2\theta$$
$$\sigma_{\theta\theta} = \frac{K_I}{\sqrt{2\pi r}}\left(\frac{3}{4}\cos\frac{\theta}{2} + \frac{1}{4}\cos\frac{3\theta}{2}\right) + \frac{K_{II}}{\sqrt{2\pi r}}\left(-\frac{3}{4}\sin\frac{\theta}{2} + \frac{3}{4}\sin\frac{3\theta}{2}\right) + T\sin^2\theta \quad (1)$$
$$\sigma_{r\theta} = \frac{K_I}{\sqrt{2\pi r}}\left(\frac{1}{4}\sin\frac{\theta}{2} + \frac{1}{4}\sin\frac{3\theta}{2}\right) + \frac{K_{II}}{\sqrt{2\pi r}}\left(+\frac{1}{4}\cos\frac{\theta}{2} + \frac{3}{4}\cos\frac{3\theta}{2}\right) - T\sin\theta\cos\theta,$$

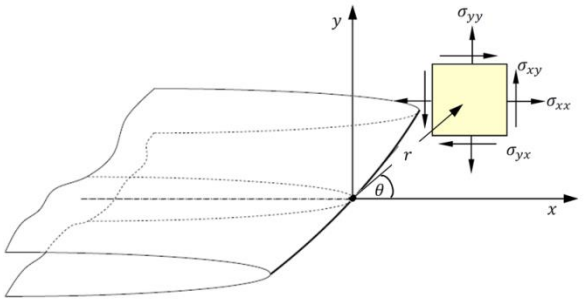

Fig. 1. Stress in a polar coordinate system ahead of a crack in an infinite plate.

where σ_{ij} is the stress tensor, r represents the distance of element from the crack tip, and θ is the angle of element with respect to a polar axes located at the crack tip. The non-singular term is known as the T-stress. Different methods have been used for calculating the T–stress term (Ayatollahi et al., 1998; Wang, 2002). Near the crack tip, where higher order terms of Williams' series expansion are negligible, T-stress can be determined along any direction where the singular term of σ_{rr} vanishes or can be set to zero by superposing with a fraction of $\sigma_{\theta\theta}$. This corresponds to different angular positions around the crack tip. For example:

$$T = (\sigma_{rr} - \sigma_{\theta\theta}) \text{ for } \theta = 0, \tag{2}$$

$$T = \sigma_{rr} \text{ for } \theta = (\pi \text{ or } -\pi). \tag{3}$$

The T-stress can also be computed by using the displacement field along the crack faces, given by:

$$u = u^{K_I} + u^{K_{II}} + u^T \qquad v = v^{K_I} + v^{K_{II}} + v^T \tag{4}$$

$$\begin{cases} u^{K_I} = \frac{K_I(1+\gamma)}{E}\sqrt{\frac{2r}{\pi}}cos\frac{\theta}{2}\left[1 - 2\gamma + sin^2\frac{\theta}{2}\right] \\ u^{K_{II}} = \frac{K_{II}(1+\gamma)}{E}\sqrt{\frac{2r}{\pi}}sin\frac{\theta}{2}\left[2 - 2\gamma + cos^2\frac{\theta}{2}\right] \\ u^T = \frac{1-\gamma^2}{E}Trcos\theta \end{cases} \quad \begin{cases} v^{K_I} = \frac{K_I(1+\gamma)}{E}\sqrt{\frac{2r}{\pi}}sin\frac{\theta}{2}\left[2 - 2\gamma - cos^2\frac{\theta}{2}\right] \\ v^{K_{II}} = \frac{K_{II}(1+\gamma)}{E}\sqrt{\frac{2r}{\pi}}cos\frac{\theta}{2}\left[-1 + 2\gamma + sin^2\frac{\theta}{2}\right] \\ v^T = -\frac{\gamma(1+\gamma)}{E}Trsin\theta \end{cases}$$

where u represents the displacement along the crack propagation direction and v is the displacement normal to the crack propagation direction. The stress intensity factors in fracture mode I and II are denoted by K_I and K_{II}, respectively. Young's modulus takes the usual E and γ is Poisson's ratio. By considering θ =-π or +π in Eq. (4), the T-stress is given by

$$T = \frac{1}{2r}E\left(u^{KI}(\theta = \pi) + u^{KI}(\theta = -\pi)\right). \tag{5}$$

In Eqns. (2, 3, 5) T-stress can be calculated directly from a finite element simulation without the need for stress intensity factors. For three-dimensional cracked specimen with finite thickness, the out-of-plane constraint effect is characterised by an additional parameter, called the T_z-factor (Matvienko et al., 2013):

$$T_z = \frac{\sigma_{zz}}{\left(\sigma_{xx} + \sigma_{yy}\right)}. \tag{6}$$

2.2. Computation of Q-factor

A dimensionless constraint parameter, Q-factor, was proposed by O'Dowd and Shih (1992) to compensate for the difference between stresses in the vicinity of any given crack and the SSY stress field by an equidistant shift. The Q-factor is described by

$$\sigma_{ij} = \sigma_{ij}^{SSY}\left(\frac{r}{J/S_y}, \theta\right) + QS_y f_{ij}(\theta), \tag{7}$$

where σ_{ij}^{SSY} denotes the stress determined from boundary layer analysis and S_y represents the yield stress of the material. The value of Q-factor depends on r and θ, and thus it is a typical practice to measure the Q-factor at θ=0 and $2\,J/S_y$<r <$5\,J/S_y$, because of the small influence from the crack seen at this distance.

In this study, a large disk shape model with a remote boundary condition controlled by K=250 MPa/$\sqrt{m}$ is used for calculating the SSY reference values. The SSY model is an elastic–plastic problem where loading is applied uniformly on the finite element model by displacement boundary conditions. The values of displacement components $u(r,\theta)$ and $v(r,\theta)$ of the SSY model were calculated by Eq. (4) and imposed at the circular boundary of the model. The radius of the model was taken to be 1 m to ensure that the SSY condition is fulfilled. Due to symmetry, only the upper-half plane was modelled. A crack was assumed as the crack-tip placed on the centre of the model. The finite element model is shown in Fig. 2. The mesh consisted of 100 centric contours focused towards the crack-tip (bias of 100000) with 100 elements in each ring. A sensitivity analysis of mesh sizes was conducted to confirm the robustness of the model.

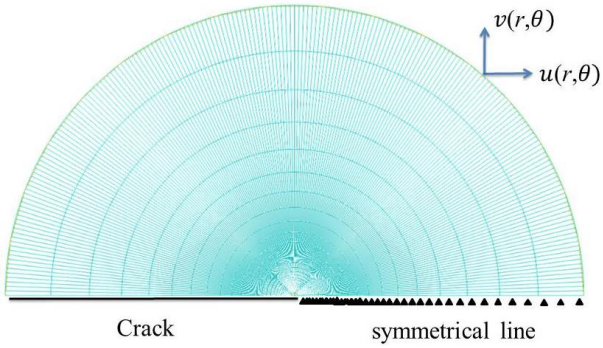

Fig. 2. SSY model with displacement boundary conditions.

The material is assumed to follow Ramberg-Osgood plasticity mode, which is

$$\frac{\varepsilon}{\varepsilon_0} = \frac{\sigma}{S_Y} + \alpha\left(\frac{\sigma}{S_Y}\right)^n, \tag{8}$$

In this study, the considered material has a strain hardening coefficient of n=10 with material coefficient α=1, and yield strength of S_Y= 400 MPa. It presents a typical moderate hardening steel commonly used internally in a nuclear reactor. The Young's modulus value of 157.85 GPa with Poisson's ratio of 0.3 were used in this study (Arun et al., 2014).

3. Finite element model description

A welded pipe made of two lengths of austenitic stainless steel joined by a girth weld was used in this study as a test specimen. A through-thickness non-symmetric circumferentially oriented pre-crack was introduced into the model. The main section of the pipe and pre-crack position are shown schematically in Fig. 3(a). The pipe has overall dimensions of 600 mm length, 180 mm outer diameter and 35 mm wall thickness. The specimen was subject to four-point bend loading. The distance between the inner loading points is 100 mm and between the outer loading points is 500 m.

Due to the symmetry, only one half of the full test specimen was modeled. Continuum elements with 8 nodes were used throughout the model. The number of elements in both the radial and circumferential directions controlled the element size. In the circumferential direction, the number of elements was set to be 8 per 45° segment, with the size in axial direction between 16 – 40 mm, whereas the number of elements in the radial direction was set to be 12 through the thickness. The total number of element generated in the model was 357,468 elements. The mesh is depicted in Fig. 3 (b).

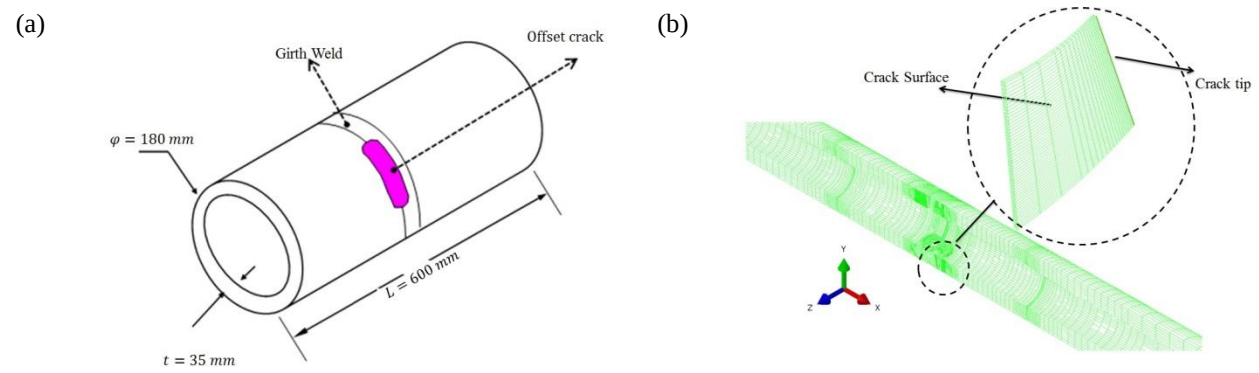

Fig. 3. (a) Schematic of welded pipe; (b) finite element model.

The residual stress was introduced directly at the integration points in the model as initial stress. Since this leads to a non-equilibrium state, an equilibrium step (static step with no additional load applied) was performed in order to obtain a self-equilibrated distribution of stresses before applying operational loads to the model. This step resulted in a difference between the initial stress input and the equilibrium residual stress obtained. To minimize this error, an iterative method was used to modify the input values of initial stress to reproduce a desired residual stress distribution in the finite element model. The adjustment equation has the form

$$\sigma|_{\text{inp}}^{i+1}=\sigma|_{\text{inp}}^{i} + \alpha\{\sigma|_{\text{M-RS}} - \sigma|_{\text{R-RS}}^{i}\} \tag{9}$$

where $\sigma|_{\text{inp}}^{i+1}$ is the initial stress input into the finite element model, $\sigma|_{\text{M-RS}}$ is the measured residual stress and $\sigma|_{\text{R-RS}}^{i}$ represent resultant residual stress obtained after an equilibrium step. The superscript in Eq. (9) represents the i-th adjustment and α is an adjustment factor, taken to be 1 here. The procedure starts with i=0, and $\sigma|_{\text{inp}}^{i}= \sigma|_{\text{M-RS}}$. After $\sigma|_{\text{R-RS}}^{i}$ is obtained from the finite element analysis, $\sigma|_{\text{inp}}^{i+1}$ is then calculated. This procedure was repeated until an agreement between $\sigma|_{\text{M-RS}}$ and $\sigma|_{\text{R-RS}}^{i}$ was obtained. The measured residual stress data for the weld pipe in a large scale bending test simulation can be found in Arun (2014).

4. Result and discussion

The determination of T-stress was done using Eqns. (2) and (3), based on stresses, and Eq. (5) based on displacements. Furthermore, Eq. (6) was programmed in Code_Aster to compute out-of-plane constraint, the T_z factor. To verify the accuracy of developed macro function, two standards test specimens were examined: (i) the single edge notched (SEN) specimen; and (ii) an elliptic crack in a three-dimensional body subject to a tensile loading. The specimens are illustrated in Fig. 4. For both test specimens the ratio of crack length a to the width W was 0.1. The value of the far-field stress, σ, was fixed to 1 MPa in both cases. Due to symmetry, only one half of the SEN and one quarter of the elliptical crack needed to be considered. Results for T/σ calculated from the stress and displacement methods for SEN and the elliptical crack specimens were obtained as -0.5603 and -1.07, respectively. For SEN, the results were within 2% of the result obtained by Ayatollahi et al. (1998). For the elliptical crack, the ABAQUS finite element package was employed with the same mesh. The results were less than 4% different. In the ABAQUS software the interaction integral method uses for calculation of the J-integral, stress intensity factors, and the T-stress. Details of T-stress computation in ABQUS is well presented by Kim and Paulino (2003).

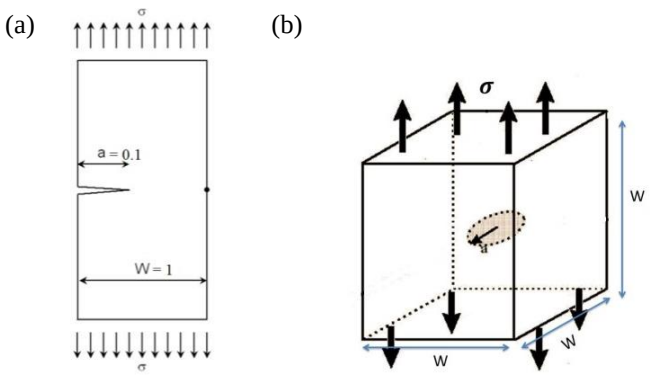

Fig 4. Single edge notched specimen (a) and (b) elliptic crack in three-dimensional body subject to a pure tensile loading.

Three dimensional finite element models of the pipe were analysed using the linear elastic material definition and the Ramberg-Osgood plasticity formulation. The crack was present in all cases, with and without residual stress. The mesh was identical for all models. Fig. 5 shows the results for T-stresses based on stress and displacement methods without residual stress. Three dimensional finite element model of the pipe was developed in the ABAQUS finite element package with the same identical mesh to comparison the results. To check the accuracy, 20 contours request in ABAQUS to determine the value of T-stress. It is seen that the stress and displacement methods give results that compare well with ABAQUS. Generally, in the elastic loading case, the values of T-stress increased from the inner surface at radius 35 mm to the outer surface at radius 90 mm. Three methods for T-stress computation are robust as the inaccuracies resulting from the calculation of the stress intensity factors is not taken into account. The results of ABAQUS presented the linear increasing of T-stress through pipe radius since the integral is taken over a domain of elements surrounding the crack and errors in local solution parameters have less effect on the evaluated quantities but in the downside the estimation may be inaccurate from the node sets at the crack front. It should be noted that in the developed macro function the size of the crack-tip elements influences the accuracy of the solutions. For larger values of r, the higher order terms in Williams' expansion become noticeable, while for small values of r, the crack tip singularity affects the results. The final values of T-stress extrapolated from 10 field values of same interval in the constant part of the results. In these methods no special crack tip elements are required and the determination of node sets for the calculation of T-stress is simpler than in the J-integral approach. The stress method, Eq. (2), provides better results over large distances compared to the other two methods, since the singular term of σ_{rr}vanishes or can be set to zero by superposing with a fraction of $\sigma_{\theta\theta}$.

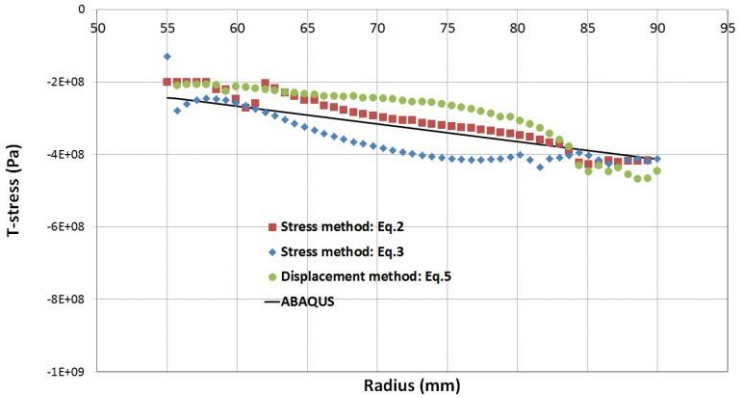

Fig 5. T-stresses pattern with different approaches without residual stress

Fig.6 shows results for T-stresses based on stress method, Eq.2, and ABQUS in the presents of residual stress. After introducing the residual stress, the T-stress along the crack front is higher by over 50% (compare Figs. 5 and 6). This is because of the combined primary and secondary loading at the crack front. The T-stress pattern still increased over pipe radius.

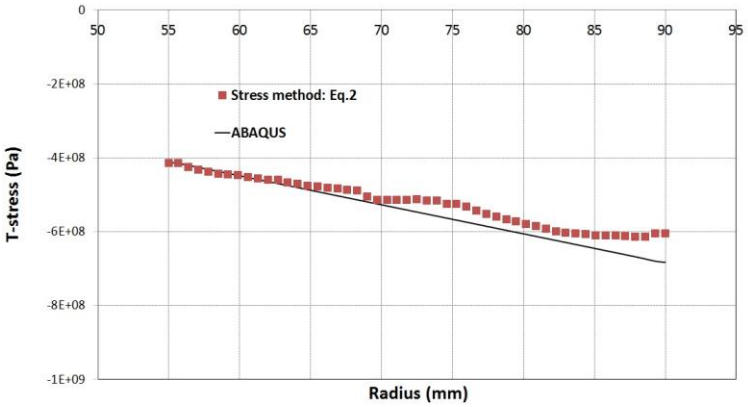

Fig 6. T-stresses pattern with stress method, Eq.2, and ABAQUS approach with residual stress

The variation of elastic constraint parameter through thickness, Tz, is presented in Fig. 7(a). It can be seen from Fig. 7(a) that the out-of-plane constraint is nearly constant throughout the pipe radius apart from the two ends. The T_z-factor equals zero at the free surfaces, depicting plane stress conditions, while the large T_z-factor within the pipe section illustrates the cause of high constraint conditions. The material along the crack surfaces, which does not yield, restrains the material ahead of the crack front causing a large build-up of stress through the thickness and, therefore, constraint. Clearly, the constraint effect in the cracked body is enhanced by the T_z-factor. Compared with the non-singular T-stress, the elastic T_z-factor describes the in-plane and out-of-plane constraint effects more realistically for the tested specimens of different configurations.

Constrain parameter Q provides a framework for quantifying the constraint as plastic flow progresses from SSY to fully yielding conditions. It was calculated for the models with and without residual stresses at distances $2< r/(J/Sy) <5$. It is worth noting that for both models, the Q-factor was found to be independent of the distance from the crack tip and a very small variation in the value of Q was observed in this range. Fig. 7 (b) presents the Q-factor against the radius in the model.

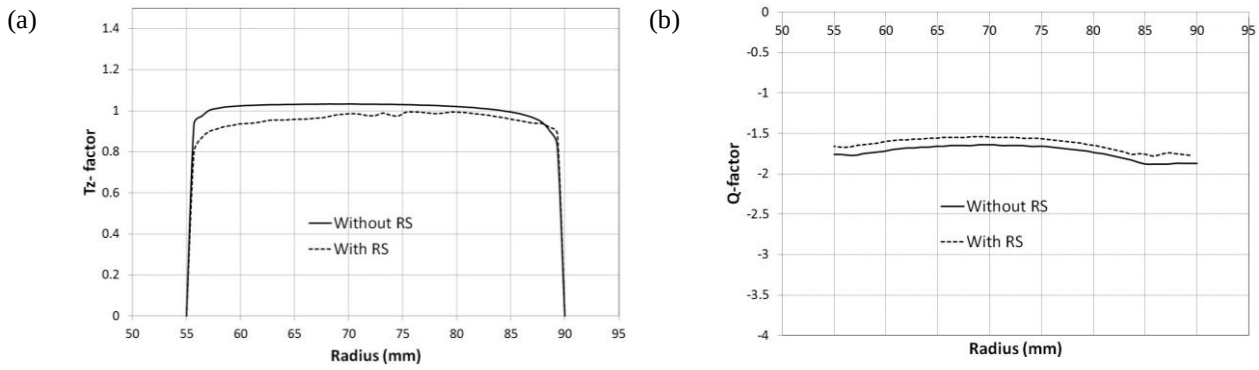

Fig 7.(a) T_z-factor; (b) Q-factor computation with and without residual stress

5. Conclusions

The in-plane and out-of-plane constraint parameters for a crack in a welded pipe are calculated with and without residual stresses. The numerical results indicate that a two-parameter fracture characterization method, K-T or J-Q, is a good approach to study the constraint effects under large scale yielding. For determining the T-stress, three methods are described based on stresses and displacements fields without having to calculate stress intensity factors. The effect of residual stresses on the elastic response increased over 50%. The Q-factor is evaluated by subtracting the stress field in the reference small-scale yielding state from the stress field in the real cracked component. All the results presented in this paper are preliminary and part of an ongoing investigation.

References

Arun, S., 2014. Finite element modelling of fracture and damage in austenitic stainless steel in nuclear power plant. PhD thesis.

Arun, S., Sherry, A.H., Smith, M.C., Sheikh, M., 2014. Finite element simulation of a circumferential through-thickness crack in a cylinder, Proceedings of the ASME Pressure Vessels & Piping Conference Anaheim, California, USA.

Ayatollahi, M.R., Pavier, M.J., Smith, D.J., 1998, Determination of T-stress from finite element analysis for mode I and mixed mode I/II loading. International Journal of Fracture, 91, 283–298.

Farahani, M., Sattari-Far, I., 2011. Effects of residual stresses on crack-tip constraints, Scientia Iranica B. 18 (6), 1267–1276.

Gannon, L., Liu, Y., Pegg, N., Smith, M., 2010. Effect of welding sequence on residual stress and distortion in flat-bar stiffened plates. Marine Structures 23 (3), 385–404.

Hill, M.R., Panontin, T.L., 1998, Effect of residual stress on brittle fracture testing, Fatigue and Fracture Mechanics. 29, 154–175 ASTM STP 1332.

Hill, M.R, Yau, T., 2000, Triaxial residual stresses affect driving force and constraint to alter fracture toughness, Proceedings of the Sixth International Conference on Residual Stresses, Oxford, UK, 1485–1492.

Kim, J.-H., Paulino, G.H., 2003. T-stress, mixed-mode stress intensity factors, and crack initiation angles in functionally graded materials: a unified approach using the interaction integral method. Computer Methods in Applied Mechanics and Engineering, 192, 1463–1494.

Liu, J., Zhang, Z.L., Nyhus, B., 2008, Residual stress induced crack-tip constraint, Engineering Fracture Mechanics 75 4151–4166.

Matvienko, Y.G., Shlyannikov, V.N., Boychenko, N.V., 2013. In-plane and out-of-plane constraint parameters along a three-dimensional crack-front stress field under creep loading. Fatigue and Fracture of Engineering Material Structure 36, 14–24.

Novotný, L., 2012, Calculation of T– stress on 3D specimens with crack. Procedia Engineering. 48, 489 – 494

O'Dowd, N.P., Shih, C.F., 1992. Family of crack-tip fields characterized by a triaxiality parameter-II. Fracture applications. Journal of Mechanics and Physics of Solids. 40, 939-963.

Wang, X., 2002, Elastic T-stress for cracks in test specimens subjected to non-uniform stress distributions, Engineering Fracture Mechanics. 69, 1339–1352.